IEEE Access
Multidisciplinary : Rapid Review : Open Access Journal

Received April 4, 2022, accepted April 23, 2022, date of publication April 28, 2022, date of current version May 6, 2022.

Digital Object Identifier 10.1109/ACCESS.2022.3171034

Compact Wideband Loop Antenna for Earbuds

TAEHYUN WOO, DONGHYUN KIM, CHAN YEONG PARK, AND YOUNG JOONG YOON, (Senior Member, IEEE)
Electrical and Electronic Engineering Department, Yonsei University, Seoul 03722, South Korea
Corresponding author: Young Joong Yoon (yjyoon@yonsei.ac.kr)

ABSTRACT This paper presents the compact wideband loop antenna with a small size of 7.05mm's radius covering ultra-wideband above 6 GHz, Wi-Fi, and Bluetooth bands for earbuds. The wide bandwidth of the proposed compact loop antenna is obtained with the antenna structure consisting of the loop antenna and the capacitive loading pin inserted in the middle of the loop antenna. The loop antenna with the capacitive loading pin supports multi-resonant modes. A wider bandwidth can be obtained by adjusting the position of the capacitive loading pin. The half-wavelength resonant frequency of the basic loop can easily be tuned through the physical capacitance between the capacitive loading pin and loop antenna. Additionally, the impedance loop is considered for the impedance matching of the compact wideband loop antenna. The simulated and measured results are included to evaluate the performance of the proposed compact wideband loop antenna. Consequently, we obtained that the simulation and measurements results are consistent.

INDEX TERMS Earbuds, hearing instruments, wearable device, ultra-wideband, loop antenna.

I. INTRODUCTION

After the Federal Communications Commission approved the operation of ultra-wideband (UWB) in February 2002, related technologies have been continuously developed [1]. UWB technology has recently been commercialized in small electronic devices such as mobile phones and accessories. The most significant advantage of UWB is that it can significantly reduce the position error indoors using a modulation-based pulse without a carrier. Through this, users can receive various advertisements and service benefits while moving. Earbuds like True Wireless Stereo (TWS) earphones are products that can maximize UWB service. It is not simply a wireless earphone connected to a mobile phone to stream music based on Bluetooth (BT), but it can be an independent accessory that gets voice services in various places. Because the Wi-Fi repeater has location information, Wi-Fi technology is essential for this indoor positioning-based UWB service. Therefore, research on UWB antennas, including a Wi-Fi band for earbuds, is necessary.

However, research on antennas for earbuds has been conducted only to cover the BT band and reduce the size [2]–[6]. It is essential to develop an advanced antenna to operate UWB and Wi-Fi band for local-based service (LBS) in earbuds. Small-sized wideband antennas have been studied to review the antennas applicable to the earbuds [7]–[18]. There are methods to Planar Inverted-F Antenna (PIFA) with slot [7], [8], slot antenna with Inverted-F Antenna (IFA), dipole, and monopole [9]–[11], appropriate design cases of feeder and slot antenna [12]–[15], and how to make additional resonant modes between the resonant modes of the loop antenna by adding a capacitance factor in the middle of the loop antenna in series [16]–[18]. Although the previously reported methods have differences in the limited ground size of the earbuds and antenna positions, it is shown that a wideband design is possible by designing a basic antenna and creating additional operation modes. Antennas that require a lot of antenna areas, such as PIFA and slots, cannot be designed in earbuds to secure the touch sensor area. Loop antennas require a wider bandwidth than previous studies; thus, a different approach is required.

This paper proposes a method to operate in UWB above 6 GHz, Wi-Fi, and BT bands by reflecting additional elements to the loop antenna in earbuds. The capacitive loading pin and ground are used to design the loop antenna for wideband performance and miniaturization. Two sub-loops are created by adding a capacitive loading pin and ground, enabling wideband design. The loop antenna with ground generates 0.5λ resonant mode to enable a miniatured loop antenna. Thus, 0.5λ, 1.0λ, 1.5λ, and 2.0λ resonant modes are implemented in the basic loop antenna; 0.5λ, and 1λ resonant modes are implemented in the sub-loop antenna to

The associate editor coordinating the review of this manuscript and approving it for publication was Davide Comite.

TABLE 1. Parameter values of the proposed antenna.

Parameter	Description	Value
W_C	Width of the capacitive loading pin	1.44mm
W_F	Width of the feeding pin	4.2mm
W_M	Width of the impedance matching pin	0.4mm
W_R	Width of the radiating loop	0.7mm
W_S	Width of the shorting pin	0.4mm
CTL	Location of capacitive loading pin ($L_{R2} - L_{R1}$)	4.4mm
G	Gap between feeding pin and shorting pin	1mm
R_R	Outermost radius of radiating loop	6.85mm
L_M	Length of the impedance matching pin	4.7mm
L_{R1}	Length from feeding pin to capacitive loading pin in radiating loop	15.85mm
L_{R2}	Length from capacitive loading pin to shorting pin in radiating loop	20.25mm
L_R	Length from feeding pin to shorting pin in radiating loop	37.54mm

TABLE 2. Wavelength according to resonant modes.

Type	operating mode (λ)	resonant frequency (GHz)	wavelength (mm)
Basic	0.5	2.45	0.4 λ_0
	1	5.13	0.9 λ_0
	1.5	6.75	1.2 λ_0
	2	8.68	1.5 λ_0
Sub1	0.5	8.25	0.8 λ_0
	1	10.67	1.1 λ_0
Sub2	0.5	5.78	0.7 λ_0
	1	9.03	1 λ_0

* λ_0 is the wavelength of resonant frequency in free space

operate eight resonant modes. These resonant modes are later verified through current distribution and impedance analysis. Broadband performance can be realized through the location of the capacitive loading pin. Additionally, the 0.5λ resonant frequency of the basic loop can easily be shifted through the physical capacitance between the capacitive loading pin and radiating loop. The impedance loop is added to match the impedance of a wideband. The proposed antenna operates UWB above 6 GHz (6-10.6 GHz), Wi-Fi (5.15-5.825 GHz), and BT (2.4-2.4835 GHz) bands. In the UWB band above 6 GHz, it operates $|S_{11}| \leq -10$ dB, which is the UWB standard for LBS use, and in the BT and Wi-Fi bands, it is designed to be $|S_{11}| \leq -6$ dB based on a small antenna for earbuds [2]–[5]. The proposed antenna is designed within a radius of 7.05 mm, considering the size of a commercial coin battery of the ultra-small earbuds. Therefore, it is suitable for earbuds and wearable devices. The performance of the proposed loop ntenna is confirmed using CST [19] and measurement.

II. GEOMETRY AND ANALYSIS OF THE PROPOSED ANTENNA

Fig. 1. shows a perspective view of the proposed antenna. The equivalent structure is illustrated in Fig. 2 to demonstrate the operation principle. The basic loop consists of a feeding pin, radiating loop, shorting pin, and ground. The sub-loops are formed by dividing the main loop through the capacitive loading pin for broadband performance. There is a physical capacitor between the capacitive loading pin and radiation loop to tune the 0.5λ resonant mode of the basic loop. The impedance matching pin is added to match the impedance of 0 ohms. The size of the circular ground has a radius of 7.05 mm, considering the size of the coin-type battery used in the earbuds. The circular ground is Taconic RF-35 substrate ($\varepsilon_r = 3.5$, loss tangent = 0.0018, and thickness = 0.5 mm). The other parts are Taconic RF-35 substrate ($\varepsilon_r = 3.5$, loss tangent = 0.0018, and thickness = 0.25 mm). Table 1 presents the parameter values of the proposed antenna.

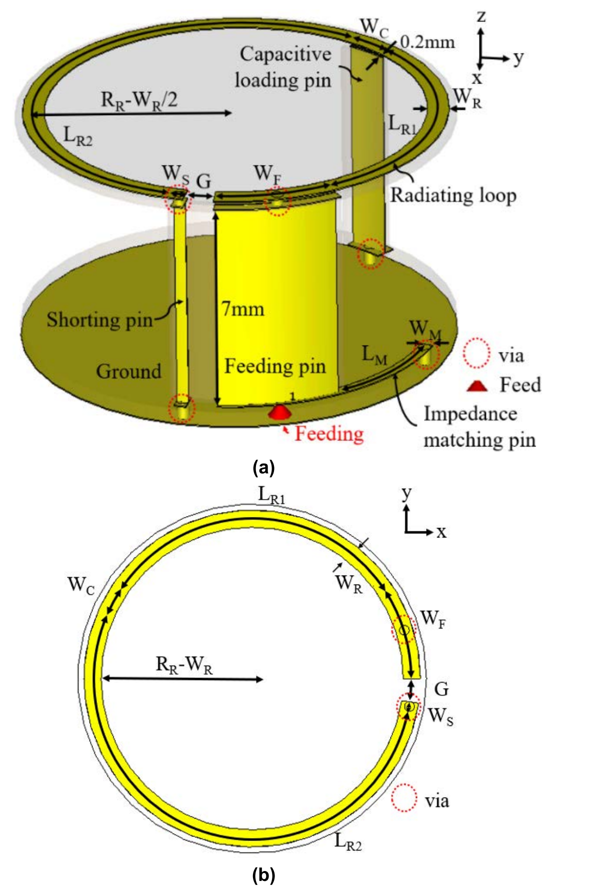

FIGURE 1. Geometry of the proposed loop antenna: (a) Perspective view, (b) Top view.

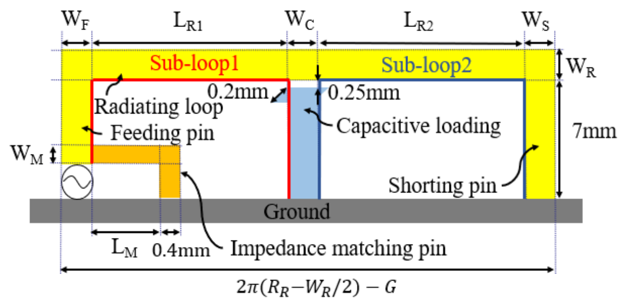

FIGURE 2. Equivalent structure of the proposed loop antenna.

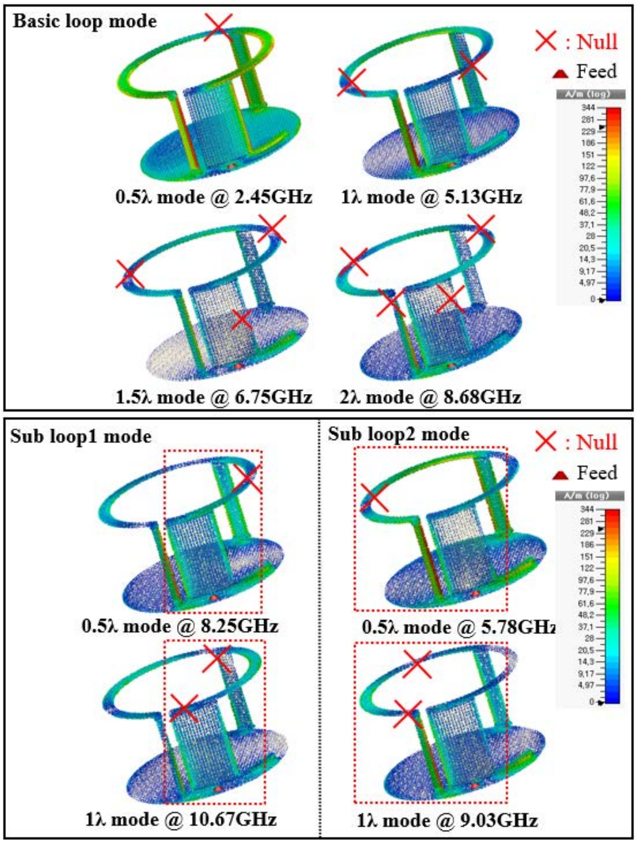

FIGURE 3. Simulated surface current distributions of eight resonances of the proposed loop antenna.

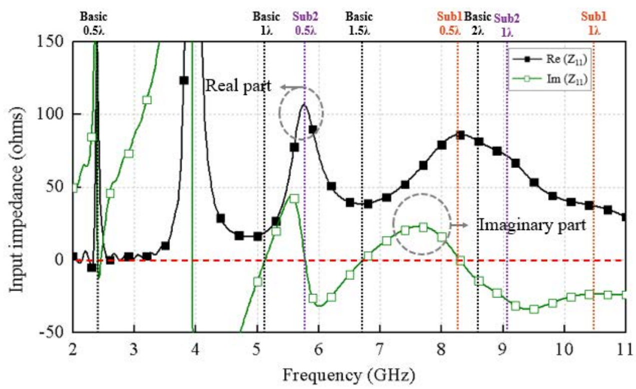

FIGURE 4. Simulated input impedance of eight resonances of the proposed loop antenna.

Fig. 3 shows the current distributions of the proposed loop antenna, where the cross "×" represents the current null point. In the basic loop, 0.5λ, 1λ, 1.5λ, and 2λ resonant modes operate, and in each sub-loop, 0.5λ and 1λ resonant modes work. Fig. 4 shows the input impedance of the proposed loop antenna. The feeding and shorting pins are perpendicular to the ground, and the radiating loop is parallel to the ground. The direction of the current changes in each mode, and the width of each pin affects the impedance.

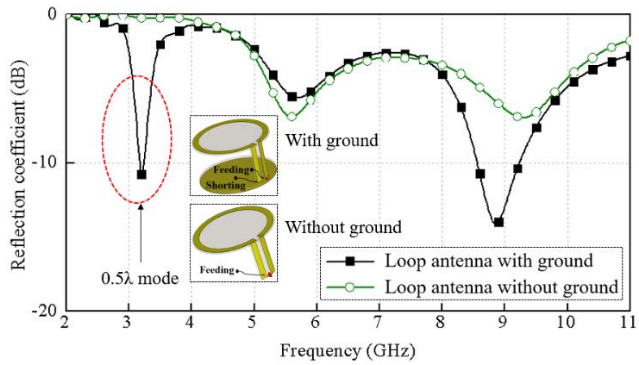

FIGURE 5. Simulated reflection coefficient of the loop antenna with effects of the ground.

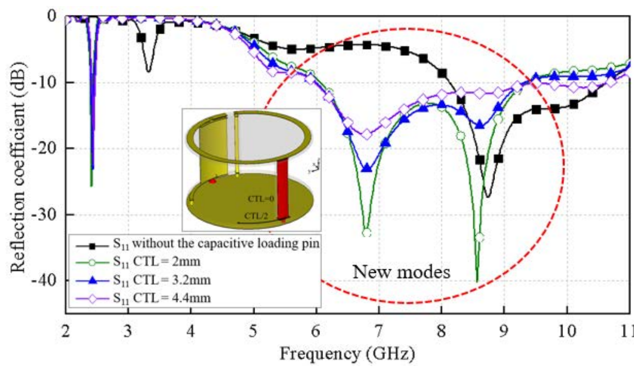

FIGURE 6. Simulated reflection coefficient of the proposed antenna with effects of the capacitive loading pin and *CTL*.

Therefore, the width of each pin is optimized to match the impedance of 50 ohms. Table 2 shows the wavelength for the operating frequency according to each operation mode. In the case of sub modes, looking at the current distribution in Fig. 3, other sub-loop and basic loop exist as parasitic components. As a result, the wavelength seems to be increased.

A. LOOP ANTENNA WITH GROUND

It is necessary to use a 0.5λ resonant mode for a miniaturized loop antenna. One way to create a 0.5λ resonant mode is using a ground [20]. The loop antenna with the ground is an unbalanced feeding structure. One end of the loop antenna is connected with the shorting pin to the ground plane, and the other end serves as the feeding point. Fig. 5 shows the ground effect of the loop antenna when the width of the loop antenna is 1 mm. Half-wavelength resonance of the loop antenna is possible due to the ground effect in the earbud model.

B. EFFECT OF THE CAPACITIVE LOADING PIN

The capacitive loading pin is used for wideband performance and moving 0.5λ resonant frequency in basic loop. Open-ended antennas such as PIFA [21], IFA [22], and dipole [23] se a capacitive loading to reduce antenna size. For loop

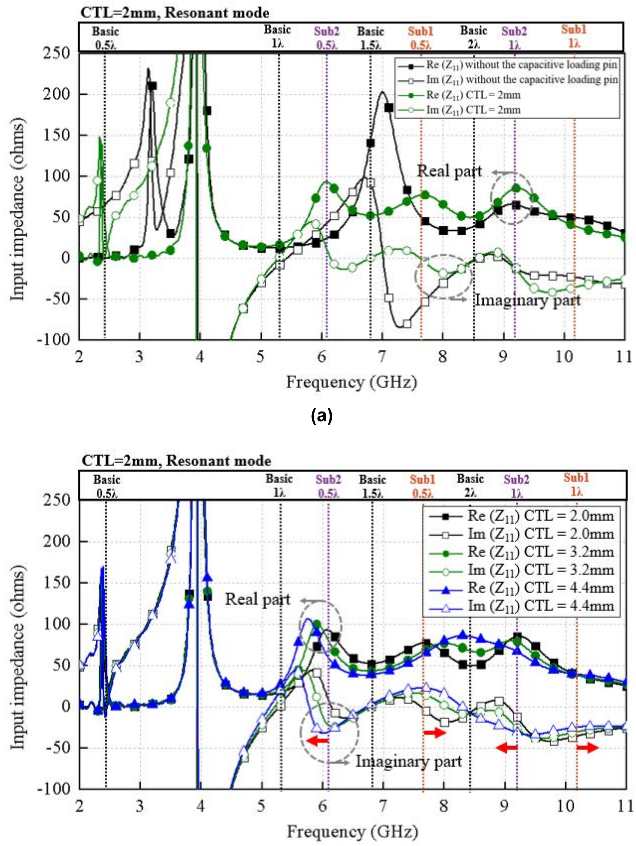

(a)

(b)

FIGURE 7. Simulated input impedance of the proposed antenna with effects of the capacitive loading pin and *CTL*: (a) comparision between a effect of the capacitive loading pin, (b) the location of the capacitive loading pin (*CTL*).

antenna, capacitive loading allows additional wideband designs. Fig. 6 shows that new resonant modes are generated when a capacitive pin is inserted. Additionally, as CTL increases, the UWB, and Wi-Fi bands become broader. CTL is the parameter for the position of the capacitive loading pin. CTL is the difference in length between the two sub-loops. L_R is the length of the radiating loop from the feeding pin to shorting pin ($L_R = 2\pi\,(R_R - W_R/2) - G - W_F - W_S$). L_{R1} is the length of the radiating loop from the feeding pin to the capacitive loading pin ($L_{R1} = (L_R - W_C)/2 - CTL/2$), and L_{R2} is the length of the radiating loop from the capacitive loading pin to the shorting pin ($L_{R2} = (L_R - W_C)/2 + CTL/2$). Fig. 7 shows the simulated input impedance to verify the new resonant modes. Fig. 7(a) shows the added resonant modes of two sub-loops created by the two sub-loops because of the capacitive loading pin. Fig. 7(b) shows that as the CTL increases, the resonant frequencies of the sub-loop1 move to a high-frequency band, whereas the resonant frequencies of the sub-loop2 move to a low-frequency band. Additionally, as the CTL value increases, the electrical length of sub-loop1 decreases, whereas the electrical length of sub-loop2 increases. Therefore, as the CTL value increases, a wider bandwidth is satisfied.

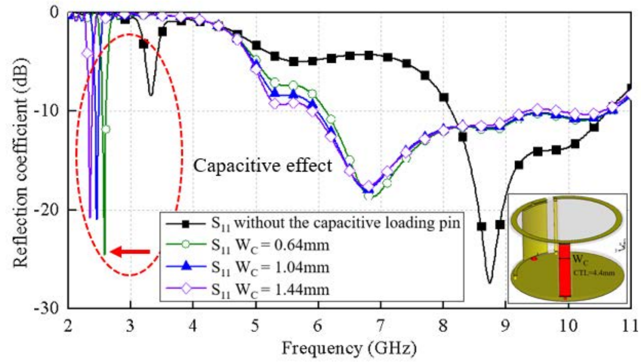

FIGURE 8. Simulated reflection coefficient of the proposed antenna with effects of the capacitive loading pin and W_C.

The loop antenna has the same current distribution as the quarter-wavelength monopole in half-wavelength mode. Therefore, when the capacitive loading pin is inserted at the midpoint of the radiating loop where the current becomes null in the half-wavelength mode of the loop antenna, the operating frequency can be moved to the lower frequency band. Thus, it is possible to satisfy the BT band without increasing the antenna's physical length. The shift of the resonant frequency is explained using Equation (1). The resonant frequency shifts to a lower frequency as the inductance and capacitance values increase.

$$f \propto \frac{1}{\sqrt{LC}} \tag{1}$$

The capacitance of physical capacitor can be expressed as follows:

$$C = \varepsilon \frac{A}{d} \tag{2}$$

where C is the capacitance, ε is the permittivity, A is the area of the capacitor, and d is the space of both plates. The spacing d of both plates is fixed 0.25 mm, which is the thickness of the PCB's substrate. The relative permittivity of the designed PCB is 3.5. Because the physical capacitor plate area is 0.2 mm$\times W_C$ mm, the half-wavelength resonant frequency of the basic loop can be adjusted through W_C. Fig. 8 shows that the resonant frequency of the half-wavelength resonant mode of the basic loop can be shifted to the BT band according to the W_C value.

C. EFFECT OF THE IMPEDANCE MATCHING PIN

IFA can easily match 50 ohms by adding one loop to the Inverted-L antenna and increasing the low input resistance by adjusting the length of the matching loop. As the length of the impedance matching decreases, the current value to the impedance matching increases, reducing the current value input to the radiation antenna. Therefore, the input resistance value entering the radiating antenna increases [24]. The technique of matching the impedance through the additional current path can also be applied to the loop antenna. Fig. 9 shows the simulated reflection coefficient

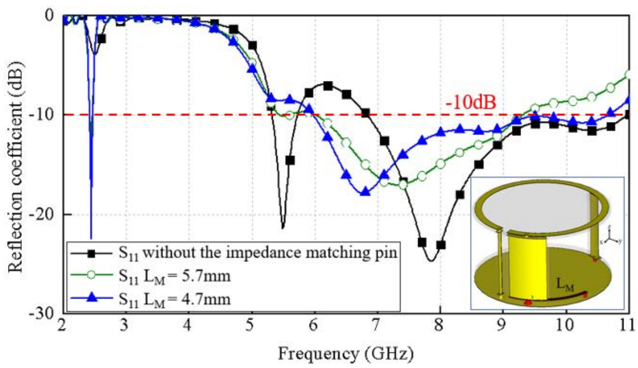

FIGURE 9. Simulated reflection coefficient of the proposed antenna with effects of the impedance matching pin and L_M.

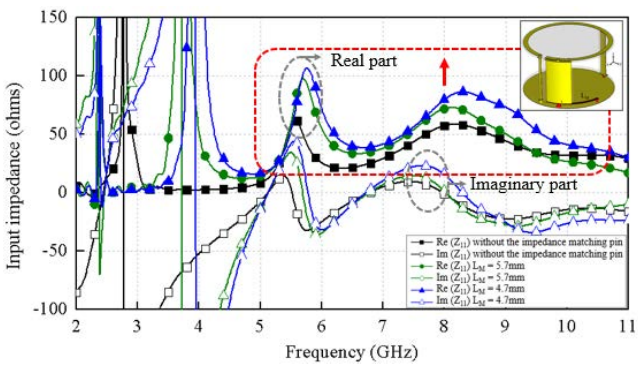

FIGURE 10. Simulated reflection coefficient of the proposed antenna with effects of the impedance matching pin and the L_M.

according to the length of the impedance matching pin. Fig. 10 shows the simulated input impedance to analyze the change in input impedance. The input resistance value increases as the length of the input impedance matching pin reduces.

III. RESULTS AND DISCUSSION

The proposed loop antenna with optimized parameters is conducted as shown in Fig. 11. The fabricated antenna is fed with a coaxial cable, as shown in Fig. 11(e).

Fig. 12 shows the simulated and measured reflection coefficients in free space (FS) and in-the-ear (ITE). Head model provided by CST is used for simulation, and EAR-A2-P10 model is used for measurement. Bandwidth is defined as $|S_{11}| \leq -6$ dB for BT and Wi-Fi, and $|S_{11}| \leq -10$ dB for UWB. The measured FS bandwidths are BW_{6dB_BT} = 90 MHz (2.47-2.56 GHz), BW_{6dB_WiFi} = 1,170 MHz (5.05-6.22 GHz), and BW_{10dB_UWB} = 2,990 MHz (6.22-8.82 GHz, 9.28-9.67 GHz). The lowest reflection coefficient value in the UWB band is −7.95 dB at 10.2 GHz. The measured ITE bandwidths are BW_{6dB_BT} = 150 MHz (2.3-2.45 GHz), BW_{6dB_WiFi} = 955 MHz (4.87-5.825 GHz), and BW_{10dB_UWB} = 3,225 MHz (5.825-9.05 GHz). The lowest reflection coefficient value in the UWB band is −5.46 dB at 10.17 GHz. Comparing the results of ITE and

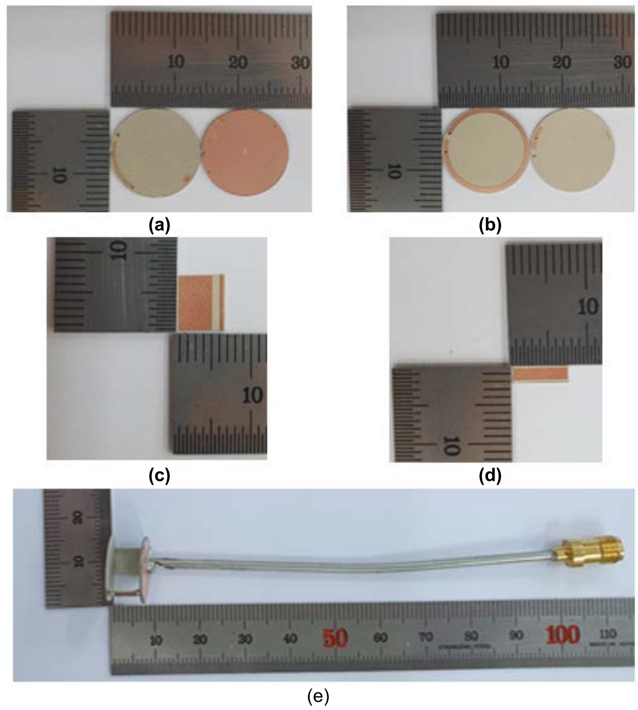

FIGURE 11. Photographs of the fabricated proposed antenna. (a) circular ground part (b) radiating loop part (c) feeding and shorting pin (d) capacitive loading pin (e) assembled prototype.

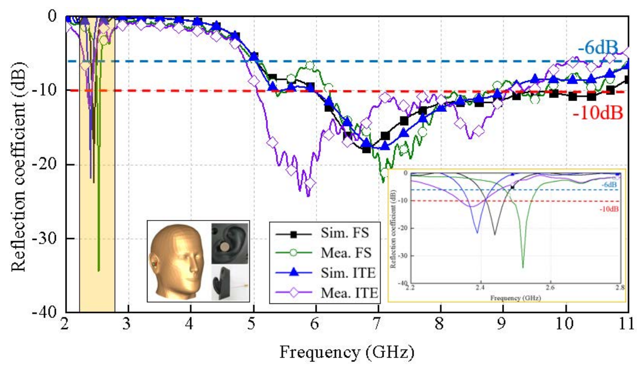

FIGURE 12. Simulated and measured reflection coefficient of the proposed loop antenna in FS and ITE.

FS conditions, the resonant frequencies move to a slightly lower frequency band due to the body effect [5]. And the measured results show the reduced bandwidth compared with the simulated results because the measurement environments such as the position of the antenna and the ear shape are not exactly matched with the simulation and there exists some minor manufacturing error due to the coaxial feeding cable.

The measured total efficiency and peak gain are plotted in Fig. 13 compared to the simulation results in FS. The simulated total efficiency is up to 49.74 % (2.45 GHz) in the BT band, 85.04 % (5.75 GHz) in the Wi-Fi band, and 97.41% (6.75 GHz) in the UWB band, respectively. The measured total efficiency is up to 78.37 % (2.55 GHz) in the BT band, 76.36 % (5.5 GHz) in the Wi-Fi band, and

TABLE 3. Performance comparison of wideband antennas.

Ref	Antenna type	Size of Antenna (L×H mm^2)	BW (GHz)	Operating bands	Total Efficiency (%)	Application
proposed	loop	37.54×7 ($0.3\lambda_L \times 0.056\lambda_L$)	2.4-2.4835 *$\|S_{11}\|_{-6dB}$ 5.15-5.825 *$\|S_{11}\|_{-6dB}$ 6-10.6 *$\|S_{11}\|_{-10dB}$	BT Wi-Fi 5 GHz UWB high band	41.78-49.74 79.45-85.04 89.06-97.41	earbuds
[7]	hybrid (PIFA& slot)	53×41.4 ($0.883\lambda_L \times 0.69\lambda_L$)	5-7 *$\|S_{11}\|_{-10dB}$	WLANs IoV	NA	vehicles
[8]	hybrid (PIFA& slot)	30×7 ($0.33\lambda_L \times 0.077\lambda_L$)	3.3-7.5 *$\|S_{11}\|_{-6dB}$	5G	40–78	smartphones
[9]	hybrid (Slot & IFA)	12.4×1.5 ($0.136\lambda_L \times 0.017\lambda_L$)	3.3-7.1 *$\|S_{11}\|_{-6dB}$	5G	49-76	smartphones
[10]	hybrid (Slot & dipole)	40×7.5 ($0.44\lambda_L \times 0.083\lambda_L$)	3.3-5.0 *$\|S_{11}\|_{-6dB}$	5G	58.9-88.6 31.6-76.7	smartphones
[11]	hybrid (Slot & monopole)	43×8 ($0.126\lambda_L \times 0.023\lambda_L$)	3.3-5 *$\|S_{11}\|_{-6dB}$	5G	63-79 61-87	smart watch
[12]	slot	15×3 ($0.165\lambda_L \times 0.033\lambda_L$)	3.3-4.2 *$\|S_{11}\|_{-6dB}$ 4.4-5 *$\|S_{11}\|_{-6dB}$ 5.15-5.925 *$\|S_{11}\|_{-6dB}$	5G	40-71	smartphones
[13]	slot	17×5.7 ($0.187\lambda_L \times 0.063\lambda_L$)	3.3-6 *$\|S_{11}\|_{-6dB}$	5G	40-90	smartphones
[14]	slot	28×7 ($0.308\lambda_L \times 0.077\lambda_L$)	3.3-5 *$\|S_{11}\|_{-6dB}$	5G	55-83.1 52.5-83.1	smartphones
[15]	slot	9×7 ($0.099\lambda_L \times 0.077\lambda_L$)	3.27-5.92 *$\|S_{11}\|_{-10dB}$	5G WLAN 5 GHz	50-82	smartphones
[16]	loop	147.7×0.8 ($1.068\lambda_L \times 0.006\lambda_L$)	2.17-2.97 *$\|S_{11}\|_{-10dB}$	NA	82-94	-
[17]	loop	50×20 ($0.35\lambda_L \times 0.14\lambda_L$)	2.1-2.9 *$\|S_{11}\|_{-10dB}$	NA	NA	mobile platforms
[18]	loop	22×6 ($0.242\lambda_L \times 0.066\lambda_L$)	3.3-5 *$\|S_{11}\|_{-6dB}$	5G	55-80	smartphones

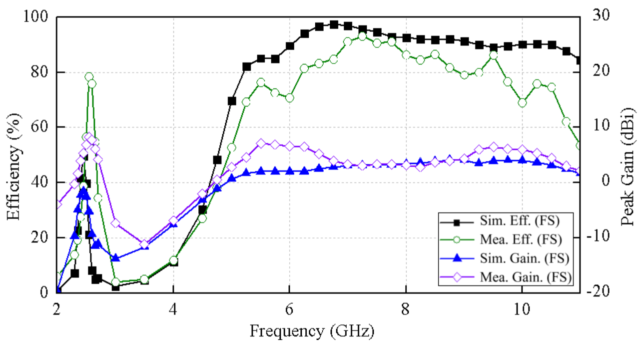

FIGURE 13. Simulated and measured total efficiency and peak gain of the proposed loop antenna.

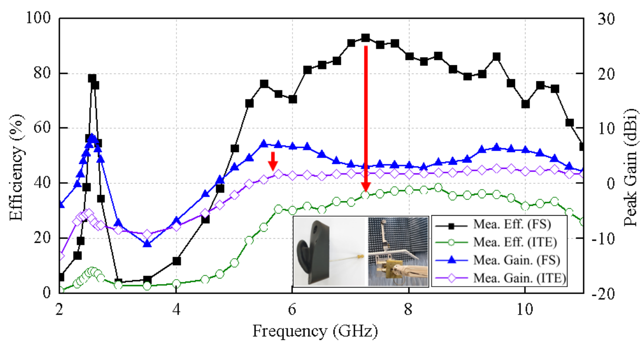

FIGURE 14. Measured total efficiency and peak gain in FS and ITE.

93.13 % (7.25 GHz) in the UWB band. The total efficiency follows the reflection coefficient results. The simulated peak gain performance is up to −1.53 dBi (BT band), 2.01 dBi (Wi-Fi band), 4.15dBi (UWB band), measured peak gain performance is up to 5.4 dBi (BT band), 7.09 dBi (Wi-Fi band), 6.61 dBi (UWB band).

Fig. 14 shows the difference in total efficiency and peak gain measured in FS and ITE. The measured total efficiency is 90.57% and 36.13% in FS and ITE at 7.5 GHz, respectively, reducing the total efficiency by about 40%. Total efficiency degradation through the human body effect is like the previous study [5]. Similarly, the measured peak gain is 6.89 dBi and 1.69 dBi in FS and ITE at 5.75 GHz, respectively, reducing the peak gain by 5.2 dB.

For LBS using UWB, an omnidirectional radiation pattern is required. Fig. 15 shows the simulated and measured radiation patterns in FS. It has an omnidirectional characteristic. This is because the loop configuration is designed to make the current distribution in the x, y, and z directions possible. Additionally, the current distribution is diversified as the resonance mode of the loop antenna changes according to the frequency. The abnormal peaks appear in the -z direction of the measured patterns due to the elongated coaxial cable which is fabricated for the ITE mode measurement.

The performance of the proposed loop antenna is compared to the wideband antennas in Table 3. Compared with reported other wideband antenna designs, the proposed loop antenna design has wideband performance and small size applications.

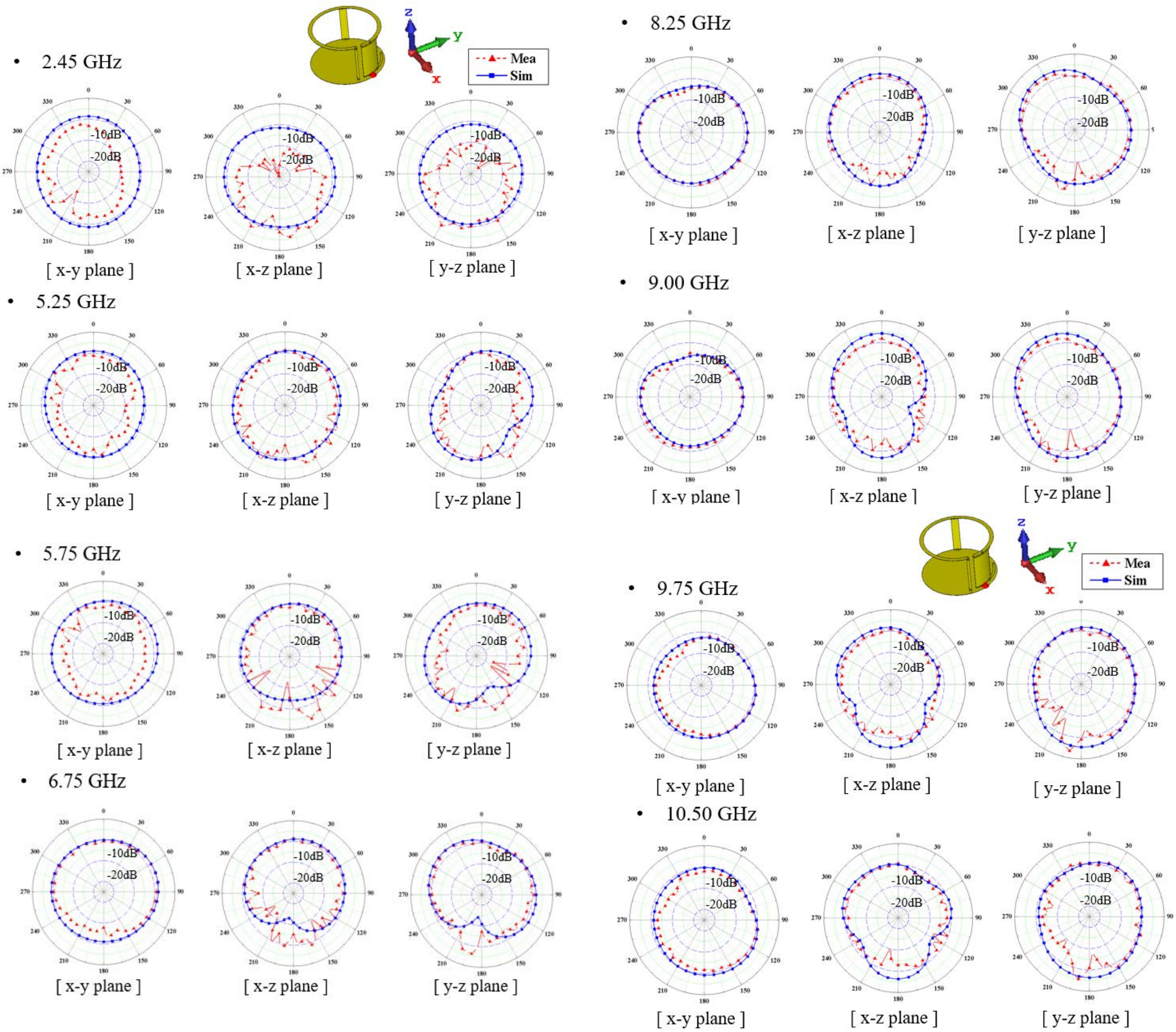

FIGURE 15. Simulated and measured radiation patterns.

IV. CONCLUSION

This paper proposes the compact loop antenna for earbuds that covers the application of UWB, Wi-Fi, and BT. It is designed to cover the application of UWB and Wi-Fi to provide an LBS in a streaming service based on simple BT communication. The proposed antenna designs a basic loop antenna on the ground and puts the capacitive loading pin in the middle to create two sub-loops. Multiple resonances can be created to ensure wideband performance by adjusting the capacitive loading pin's position to tune the sub-loop antenna's length. The capacitor for capacitive loading is physically designed. The capacitive effect can be controlled by adjusting the area of the physical capacitor. Consequently, the frequency of the 0.5λ resonant mode of the basic loop can work at BT band. The impedance matching loop can be added to match low impedance to high impedance. The impedance matching loop is in the minimum area of PCB used as ground. The proposed loop antenna is designed in a very small size. Therefore, it is suitable for earbuds and other wearable devices.

REFERENCES

[1] *Federal Communications Commision Revision of Part 15 of the Commision's Rules Regarding Ultra-Wideband Transmission System From 3.1 GHz to 10.6 GHz*, 2002, pp. 98–153.

[2] N. P. I. Kammersgaard, S. H. Kvist, J. Thaysen, and K. B. Jakobsen, "In-the-ear spiral monopole antenna for hearing instruments," *Electron. Lett.*, vol. 50, no. 21, pp. 1509–1511, Oct. 2014.

[3] W. H. Yatman, L. K. Larsen, S. H. Kvist, J. Thaysen, and K. B. Jakobsen, "In-the-ear hearing-instrument antenna for ISM-band bodycentric ear-to-ear communications," in *Proc. Loughborough Antennas Propag. Conf. (LAPC)*, 2012, pp. 1–4.

[4] L. Huitema, S. Sufyar, C. Delaveaud, and R. D'Errico, "Miniature antenna effect on the ear-to-ear radio channel characteristics," in *Proc. 6th Eur. Conf. Antennas Propag. (EuCAP)*, Mar. 2012, pp. 3402–3406.
[5] A. Ruaro, J. Thaysen, and K. B. Jakobsen, "Wearable shell antenna for 2.4 GHz hearing instruments," *IEEE Trans. Antennas Propag.*, vol. 64, no. 6, pp. 2127–2135, Jun. 2016.
[6] S. H. Kvist, K. B. Jakobsen, and J. Thaysen, "Design and measurement of a 2.45 GHz on-body antenna optimized for hearing instrument applications," in *Proc. 34th Annu. Antenna Meas. Techn. Assoc. Symp. (AMTA)*, 2012, pp. 33–37.
[7] R. Jian, Y. Chen, and T. Chen, "A low-profile wideband PIFA based on radiation of multiresonant modes," *IEEE Antennas Wireless Propag. Lett.*, vol. 19, no. 4, pp. 685–689, Apr. 2020.
[8] T. Yuan, Z. Chen, T. Gu, and T. Yuan, "A wideband PIFA-pair-based MIMO antenna for 5G smartphones," *IEEE IEEE Antennas Wireless Propag. Lett.*, vol. 20, no. 3, pp. 371–375, Mar. 2021.
[9] Q. Cai, Y. Li, X. Zhang, and W. Shen, "Wideband MIMO antenna array covering 3.3–7.1 GHz for 5G metal-rimmed smartphone applications," *IEEE Access*, vol. 7, pp. 142070–142084, 2019.
[10] L. Sun, Y. Li, Z. Zhang, and Z. Feng, "Wideband 5G MIMO antenna with integrated orthogonal-mode dual-antenna pairs for metal-rimmed smartphones," *IEEE Trans. Antennas Propag.*, vol. 68, no. 4, pp. 3494–3503, Apr. 2020.
[11] C. T. Liao, Z. K. Yang, and H. M. Chen, "Multiple integrated antennas for wearable fifth-generation communication and Internet of Things applications," *IEEE Access*, vol. 9, pp. 120328–120346, 2021.
[12] X. Zhang, Y. Li, W. Wang, and W. Shen, "Ultra-wideband 8-port MIMO antenna array for 5G metal-frame smartphones," *IEEE Access*, vol. 7, pp. 72273–72282, 2019.
[13] X. T. Yuan, W. He, K. D. Hong, C. Z. Han, Z. Chen, and T. Yuan, "Ultra-wideband MIMO antenna system with high elementisolation for 5G smartphone application," *IEEE Access*, vol. 8, pp. 56281–56289, 2020.
[14] L. Sun, Y. Li, and Z. Zhang, "Wideband decoupling of integrated slot antenna pairs for 5G smartphones," *IEEE Trans. Antennas Propag.*, vol. 69, no. 4, 2386-2391, Sep. 2020.
[15] H. D. Chen, Y. C. Tsai, C. Y. D. Sim, and C. Kuo, "Broadband eightantenna array design for sub-6 GHz 5G NR bands metal-frame smartphone applications," *IEEE IEEE Antennas Wireless Propag. Lett.*, vol. 19, no. 7, pp. 1078–1082, Jul. 2020.
[16] K. Wei, Z. Zhang, and Z. Feng, "Design of a wideband horizontally polarized omnidirectional printed loop antenna," *IEEE Antennas Wireless Propag. Lett.*, vol. 11, pp. 49–52, 2012.
[17] X. Zhao, B. N. Tian, S. P. Yeo, and L. C. Ong, "Wideband segmented loop antenna with dual-polarized omnidirectional patterns for mobile platforms," *IEEE Trans. Antennas Propag.*, vol. 65, no. 2, pp. 883–886, Feb. 2017.
[18] A. Zhao and Z. Ren, "Wideband MIMO antenna systems based on coupled-loop antenna for 5G N77/N78/N79 applications in mobile terminals," *IEEE Access*, vol. 7, pp. 93761–93771, 2019.
[19] (2019). *CST STUDIO SUITE*. [Online]. Available: https://www.cst.com
[20] Z. Zhang, *Antenna Design for Mobile Devices*. Hoboken, NJ, USA: Wiley, 2017.
[21] C. R. Rowell and R. D. Murch, "A capacitively loaded PIFA for compact mobile telephone handsets," *IEEE Trans. Antennas Propag.*, vol. 45, no. 5, pp. 837–842, May 1997.
[22] L. Loizou, J. Buckley, M. Belcastro, J. Barton, B. O'Flynn, and C. O. Mathuna, "Miniaturized inverted-F antenna with capacitive loading," in *Proc. 6th Eur. Conf. Antennas Propag. (EuCAP)*, 2013, pp. 3213–3216.
[23] S. Dakhli, M. Smari, J. Floc'h, and F. Choubani, "Design of frequency-reconfigurable triband dipole antenna using capacitive loading," in *Proc. Int. Wireless Commun. Mobile Comput. (IWCMC)*, Jun. 2020, pp. 1342–1346.
[24] W. Lee, M. Ko, J. Kim, and Y. J. Yoon, "Analysis of the shorting pin effects on an inverted-F antenna using a equivalent model for impedance matching," in *Proc. 4th Eur. Conf. Antennas Propag. (EuCAP)*, Apr. 2010, pp. 1–5.

TAEHYUN WOO received the B.S. degree in electronic engineering from Dongguk University, Seoul, South Korea, in 2008, and the M.S. degree in electrical and electronic engineering from Yonsei University, Seoul, in 2022. He is currently a Senior Researcher with the Samsung Electronics Wearable Research and Development Group. His research interests include small and mobile antennas.

DONGHYUN KIM received the B.S. degree in radio engineering from Chungnam National University, Daejeon, South Korea, in 2018. He is currently pursuing the Integrated M.S. and Ph.D. degrees in electrical and electronic engineering with Yonsei University, Seoul. He has been a Research Assistant with Yonsei University, since 2018, where he has worked on antenna development for electronic warfare. His research interests include direction finding and metamaterial.

CHAN YEONG PARK received the B.S. degree in electronic engineering from Seokyeong University, Seoul, South Korea, in 2019. He is currently pursuing the Integrated M.S and Ph.D. degrees in electrical and electronic engineering with Yonsei University, Seoul. He has been a Research Assistant with Yonsei University, since 2019, where he has worked on antenna development for mm-wave applications. His research interests include holographic antenna and metasurface.

YOUNG JOONG YOON (Senior Member, IEEE) received the B.S. and M.S. degrees in electronics engineering from Yonsei University, Seoul, South Korea, in 1981 and 1986, respectively, and the Ph.D. degree in electrical engineering from the Georgia Institute of Technology, Atlanta, GA, USA, in 1991. From 1992 to 1993, he worked as a Senior Researcher at the Electronics and Telecommunications Research Institute, Daejeon, South Korea. He joined as a Faculty Member at Yonsei University, in 1993. In 2011, he was the President of the Korean Institute of Electromagnetic Engineering and Science, Seoul. He is currently a Professor with the Department of Electrical and Electronics Engineering, Yonsei University. His research interests include high-power antennas, reflectarray, hyperthermia systems, biomedical antennas, and array antennas.